

# Journal of Materials Chemistry C

Accepted Manuscript



This is an *Accepted Manuscript*, which has been through the Royal Society of Chemistry peer review process and has been accepted for publication.

*Accepted Manuscripts* are published online shortly after acceptance, before technical editing, formatting and proof reading. Using this free service, authors can make their results available to the community, in citable form, before we publish the edited article. We will replace this *Accepted Manuscript* with the edited and formatted *Advance Article* as soon as it is available.

You can find more information about *Accepted Manuscripts* in the [Information for Authors](#).

Please note that technical editing may introduce minor changes to the text and/or graphics, which may alter content. The journal's standard [Terms & Conditions](#) and the [Ethical guidelines](#) still apply. In no event shall the Royal Society of Chemistry be held responsible for any errors or omissions in this *Accepted Manuscript* or any consequences arising from the use of any information it contains.

# Emitters as probes of a complex plasmophotonic mode

Pierre Fauché,<sup>a</sup> Simona Ungureanu,<sup>a</sup> Branko Kolaric<sup>b</sup> and Renaud A. L. Vallée<sup>\*a</sup>

Received Xth XXXXXXXXXX 20XX, Accepted Xth XXXXXXXXXX 20XX

First published on the web Xth XXXXXXXXXX 200X

DOI: 10.1039/b000000x

We report on the experimental observation of an asymmetric wavelength-dependence of the emission rate enhancement in a two-dimensional plasmophotonic crystal. This feature strongly contrasts with the traditional Lorentzian line shape exhibited at a resonance by the Purcell factor. The unusual dispersive behavior is shown to be reproducible for different combinations of emitters and structures measured in different geometries. It is further retrieved from finite-difference time-domain simulations and is dominantly attributed to the fact that a hybridized mode, resulting from the coupling of a Bragg and a surface plasmon polariton modes, is coupled to the emitters. Further studies of the emission detuning by hybrid plasmonic/photonic structures are expected to benefit many related fields and notably sensing and biosensing technologies.

## 1 Introduction

The spontaneous decay rate of a quantum emitter is strongly altered by its surrounding environment. The Purcell effect<sup>1</sup> represents the maximum spontaneous rate enhancement for an ideal coupling between a single emitter and a cavity mode, i.e., a perfect spectral, spatial, and polarization matching<sup>1</sup>. A spectral mismatch between the dipole frequency and the cavity resonance reduces the decay rate according to the usual Lorentzian line shape. It is one of the most fundamental effects investigated in quantum electrodynamics. Owing to recent advances in nanotechnology, tremendous applications have emerged and numerous fundamental studies have arisen in order to push the reachable limits of this factor. The control of spontaneous emission by manipulating optical modes with photonic crystals (PCs) has been predicted and achieved in various structures<sup>2–6</sup>. One has recently seen the advent of nanolasers<sup>7</sup>, plasmonic antenna for light<sup>8,9</sup>, plasmon based nanolasers<sup>10,11</sup>, enhanced single-photon sources<sup>12</sup>.

A hybrid optical nanocavity, consisting of a photonic crystal coupled to a metal surface separated from the PC by a nanoscale air gap, has been shown to open up opportunities for various applications in enhanced light-matter interactions<sup>13</sup>. When two-dimensional (2D) photonic crystals are made of noble metal (thereby avoiding oxidation), the periodically modulated complex dielectric function of the metallic structures allows for the optical excitation of surface plasmon polaritons (SPPs). These SPPs propagate along the metallodielectric interface due to diffractive coupling<sup>14,15</sup>. Quantum emitters located in the vicinity of such 2D metallic PCs will experience the Purcell effect<sup>16–18</sup>. Their emission can also be spectrally reshaped<sup>19</sup> or spatially redirected<sup>20,21</sup>. Such plasmophotonic systems can also be used in biosensing<sup>22,23</sup>, photovoltaic and photocatalytic devices<sup>24,25</sup>.

Actually, structures possessing a large area are beneficial to real life photonic and optoelectronic applications. Nanosphere lithography (NSL) has been used to fabricate large plasmophotonic structures<sup>26–30</sup>. In NSL, convective self-assembly (CSA) produces arrays of colloidal spheres as templates for 2D plasmophotonic architectures. Their optical properties are usually characterized by the excitation of i) non-dispersive localized surface plasmon polaritons modes (LSPPs), ii) photonic modes as the Rayleigh-Wood mode and iii) traveling SPPs, which can be excited via momentum transfer of a reciprocal lattice vector, the so-called Bloch-SPP or Bragg-plasmon (BP) mode<sup>18,31–34</sup>.

In this paper, we use NSL to engineer 2D hybrid colloidal crystals, here after named 2Dhcc structures. Owing to experimental and numerical observations of the UV-visible spectra, we assign unambiguously the transmission maximum of the structure to a BP mode. After dispersing a solution of quantum dots with their emission spectrum spectrally overlapping the BP mode of the 2Dhcc structure, we show that the average emission rate enhancement  $\langle F \rangle$  exhibits an asymmetric (non Lorentzian) dispersive behavior with an increase (decrease) of  $\langle F \rangle$  as a function of wavelength while reaching (passing over) the BP peak. This asymmetric spectral detuning between the emitter and the BP resonance is further retrieved from numerical simulations of the emission rate enhancement. It is explained in terms of hybridized mode and spatial averaging, bringing the system far from the Purcell regime. While the absolute values of  $\langle F \rangle$  are not as spectacularly large as those reported for other structures<sup>35</sup>, the observed behavior is well reproduced for different combinations of emitters and structures, pointing to the robustness of our approach.

## 2 Materials and methods

Latex micro-spheres [diameters  $D = 457$  nm and  $D = 505$  nm, 2.5% solids (w/v) aqueous suspensions] were supplied by Polysciences. Au (99.999%, 3mm x 6mm) was purchased from Neyco. CdSe@ZnS quantum dots suspended in toluene with emission peaks at either 570 nm, 610 nm and 640 nm were supplied by Aldrich. Glass plates with a size of 2X2 cm<sup>2</sup> and a thickness of 5 mm were carefully cleaned and treated with UV-ozone for 30 min. Then an opportune ratio of Triton 10 – 3 (mass) in water/polystyrene (PS) micro-spheres was deposited on the glass surface and dried under a tilt angle of approximately 10° under controlled conditions of temperature and humidity ( $T = 293$  K,  $H = 65$  %). After formation of large areas of well-ordered mono-layers of latex nano-spheres, the substrates were covered with 50 nm of gold by using a Boc-Edwards Auto306 evaporator. The thickness was controlled by an in-situ mounted quartz crystal micro-balance. Then a 20  $\mu$ l volume of QDs solution (1 % v/v in either water or toluene/ethanol) were randomly spread (drop casted) on the gold coated mono-layers. We estimated that  $\approx 10^4$  QDs were deposited on each gold coated PS bead. The AFM image of drop casted QDs on a similar hybrid plasmonic-photonic structure is published elsewhere<sup>18</sup>.

Scanning electron micro-graphs (SEM) were recorded on a field-emission scanning electron microscope (FESEM, JEOL JSM-6700F). The transmission spectra of the plasmo-photonic crystals were measured on the whole visible range, collecting the signal from a large (3 mm) area owing to a white light illumination lamp (fiber coupled white light HL-2000-HP-FHSA, Ocean Optics) used in combination with a spectrometer (fiber spectrometer USB2000 + VIS-NIR, Ocean Optics). The spontaneous emission properties of the various quantum dots were recorded with a spectral- and time- resolved set-up consisting of a streak camera (HAMAMATSU Streak Scope C10627) pre-fitted with a spectrograph (Princeton Instruments) with a 150 gr/mm choice of the grating. The excitation light was the frequency doubled output of the  $\lambda = 1030$  nm wavelength, 10 MHz repetition rate, 300 fs line width pulses delivered by a diode-pumped Ytterbium femtosecond oscillator from Amplitude systems (t-Pulse 200). The beam was collimated to a 1.5 mW, 100  $\mu$ m diameter spot to excite the emitters in the targeted nano-structure prior to focus the 530nm long-pass filtered emission intensity on the entrance slit of the spectrograph.

The transmission (T), reflection (R) and absorption (A) spectra, the modes and the local density of states of the 2Dhcc structures have been simulated by solving Maxwell equations using the three-dimensional finite-difference time-domain (FDTD) method, as implemented in the freely available MEEP software package<sup>36</sup>. By Fourier transforming the response to a short, broadband, spatially extended Gaussian pulse in the far-field of the structures and normalizing with the response of a refer-

ence (the glass substrate) for the same excitation conditions, a single simulation yielded the T, R, A spectra over a wide spectrum of frequencies. The resonance modes were obtained by sending a narrow-band, frequency gated, and spatially extended Gaussian pulse in the far-field of the structure and recording the three components of the electric field in time. Finally, in order to compute the emission rate enhancement of the emitters on the nano-structures, we performed Fourier transforms of the response to an impulsive point-dipole TM-polarized source. We then normalized this response with the one obtained for a point-dipole source located near the substrate in the same excitation conditions. In all types of simulations, the wave-vector is normal to the substrate's surface; periodic boundary conditions were implemented laterally while perfectly matched layers were implemented longitudinally, in the propagation direction. The dielectric permittivities of the glass substrate and the PS spheres were taken as 2.3 and 2.5, respectively. The dielectric permittivity of gold was specified by using a sum of Drude and Drude-Lorentz terms, according to the work performed by Rakic et al.<sup>37</sup>

## 3 Results and discussion

Mono-layers of polystyrene (PS) beads of either 457 nm or 505 nm have been self-assembled in a compact hexagonal lattice onto a glass substrate according to well-reported procedures<sup>27–29</sup>. Subsequently, these structures have been coated with a 50 nm thick layer of gold, forming 2-dimensional hybrid colloidal crystals (2Dhcc, Figure 1: the middle inset shows a scheme of the engineering process). This manufacturing technique, called Nano-Sphere Lithography, is known to allow for the easy, inexpensive fabrication of high quality, large (cm<sup>2</sup>) surface areas. Figure 1 exhibits such a large area of 100 $\mu$ m X 100 $\mu$ m with a single crystalline plane of coated beads. As a close inspection reveals, a single crystalline orientation is found from the top left of the figure to the bottom right. If some very slight grooves are frequently visible between two adjacent lines of beads (either caused by attractive capillary forces acting at a late stage of drying or by the presence of a tiny or a big bead slightly disturbing the arrangement, see the bottom left inset recorded at larger magnification), they do not reach the state of dislocations, or grain boundaries, as there are no orientation changes between adjacent domains.

The UV-visible-near IR optical properties of these 2Dhcc structures have been extensively studied in the literature<sup>18,31–33</sup>. Here, we aim to focus specifically on the BP mode, and investigate in detail its action on the emission of quantum weakly-coupled excitons. In order to precisely locate the resonance wavelength of this mode, we firstly performed transmission and reflection measurements. Figure 2a shows such spectra for a structure based on  $D = 457$  nm diameter PS beads. The absorption spectrum, also shown in Fig. 2a, has been ob-

## 3 RESULTS AND DISCUSSION

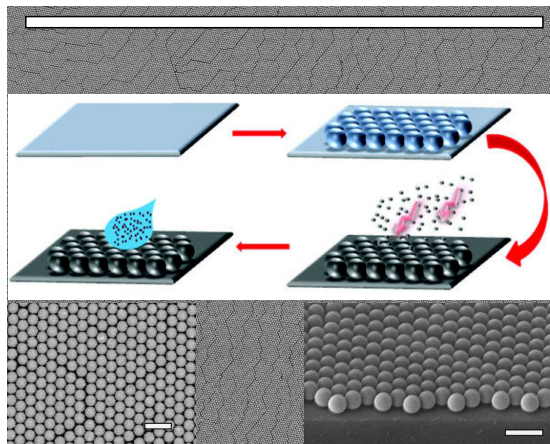


**Fig. 1** SEM micrograph of the 2D hybrid colloidal crystal (2Dhcc) recorded at low magnification (the scale bar is  $100\mu\text{m}$  long). The bottom left inset shows a portion of this micrograph obtained at larger magnification (scale bar of  $1\mu\text{m}$ ). The bottom right inset shows a tilted SEM view, evidencing the formation of a single monolayer during this assembling process. The middle inset shows a scheme of the manufacturing process, consisting in the convective self-assembly (CSA) of an hexagonal mono-layer of polystyrene (PS) beads onto a glass substrate, followed by the evaporation of a thin metal layer (50 nm) and the deposition of CdSe@ZnS quantum emitters.

tained by applying the usual formula  $A(\lambda) = 1 - T(\lambda) - R(\lambda)$ . In excellent agreement with the literature<sup>34</sup>, a major peak is observed in transmission at 610 nm, which is attributed to the BP mode. On the long wave side of this peak, a significantly reduced transmission, associated with an absorption maximum, is noticed, which can be assigned to a LSPP mode. In order to assess the quality of our samples (in addition to the SEM inspection performed in Fig. 1) and the spectral measurements, we performed FDTD simulations of transmission (T), reflection (R), and absorption (A) spectra. These far-field spectra are shown in Fig. 2b (dashed, dash-dotted, and dotted lines, respectively). Clearly, the matching of the Bragg-plasmon resonance wavelength is good between simulations and experiments. The transmission maximum is recovered, centered at 595 nm and coincides with the minimum absorption. This contrasts with the simultaneous observation of transmission and absorption maxima in extraordinary transmission of hole arrays<sup>38</sup>. Concerning the LSPP resonance wavelength, we observe a slight discrepancy between simulations and experiments, which might originate from an imperfect coverage of the gold over-layer in the experiments, as compared to the ideal simulated case.

The simulated  $H_y$  and  $E_z$  near-field patterns at the transmission maximum, TM-excited at normal incidence, are shown as insets of Fig. 2a. The  $H_y$  field is directly transmitted through the structure. The field distribution suggests that an interference mechanism (like in planar thin films) contributes to the

transmitted band. The  $E_z$  map exhibits a periodic pattern in the x direction, indicative of a propagative mode in the plane of the array, with z-polarized light propagating along the x direction. The distance between the two lobes, about half the sphere diameter, together with the large spatial extension, support the propagative nature of this mode. The same  $E_z$  map reveals a symmetric coupling between the outer and inner surfaces of the shells, again characteristic for long-range propagative modes. These features ascertain the Bragg-plasmon character of the maximum transmission peak<sup>34,39</sup>. The significant reduction of the transmission on the long wave side (Fig. 2b) coincide with an absorption maximum at 660 nm, which further signals the attribution of this mode to a LSPP<sup>34</sup>.

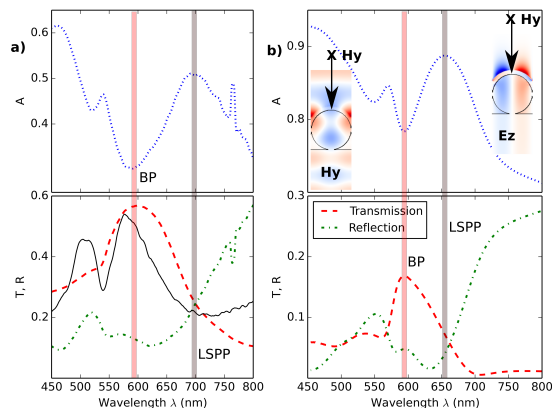


**Fig. 2** Experimental (a) and simulated (b) transmission (T, red dashed), reflection (R, green dash-dotted) and absorption (A, blue dotted) spectra of the 2Dhcc structure coated with a gold thin layer. The reflection spectrum of the bare PS monolayer assembled on the glass substrate is shown for comparison (solid black line). The insets in b) are the  $H_y$  and  $E_z$  near-field patterns of the 2Dhcc structure TM-excited at the 595 nm wavelength of the BP mode. Light is propagating from top to bottom (z-direction).

Let us now proceed to the investigation of the emission properties of QDs spread onto the structure and spectrally overlapping the BP mode. We aim to observe the spectral detuning of the emission rate enhancement between the emitter and BP resonances. An obvious way to achieve this is to i) disperse onto the structure QDs possessing an emission spectrum slightly detuned (on the long wave side) with respect to the transmission maximum, at normal incidence; ii) rotate the sample so that the maximum transmission peak is brought through the emission spectrum of the emitters. Indeed, owing to an increase of the incidence angle, the main transmission peak is expected to shift to the long wave side, going all the way through the other edge of the emission spectrum, according to the Bragg-plasmon law<sup>31,40</sup> (Eq. 1).

$$\lambda = \frac{\sqrt{3}D}{2} (\sqrt{\epsilon_{eff}(\lambda) + \sin^2\theta}) \quad (1)$$

where  $D = 457\text{nm}$  is the diameter of spheres,  $\epsilon_{eff}$  is the effective permittivity expressed by the plasmonic-dielectric interface mixing rule  $\frac{1}{\epsilon_{eff}(\lambda)} = \frac{1}{\epsilon_{Au}(\lambda)} + \frac{1}{\epsilon_{dielectric}}$ <sup>21</sup>, in which  $\epsilon_{dielectric}$  is defined on a filling factor basis  $\epsilon_{dielectric} = \epsilon_{PS}f + \epsilon_{air}(1-f)$  as estimated in ref.<sup>31</sup>.

The 610 nm maximum CdSe@ZnS emitter has precisely its emission spectrum slightly red-shifted with respect to the maximum transmission of the BP mode, at normal incidence (Fig. 4a). Figure 3b shows the 2D (x- and y-axis: spectral and temporal dimensions, respectively) fluorescence diagram measured for such  $\lambda_{max} = 610\text{ nm}$  CdSe@ZnS emitters deposited on the 2Dhcc structure at an incidence angle  $\theta = 60^\circ$  (inset). We retrieve the total decay profile, Fig. 3a, by projecting this 2D plot on the y-axis. The decay profiles are obtained as a function of wavelength by dividing the x-axis in 5 nm range windows and projecting the resulting diagrams on the y-axis. We then determine the average decay times by performing stretched exponential fits<sup>16</sup> on all 5 nm wavelength-resolved decay profiles. The profiles shown in Fig. 3c provide a direct comparison of the decay rates exhibited by the emitters deposited on either the glass substrate (reference, blue circles) or the structured sample (red triangles), in the selected wavelength range  $620\text{ nm} < \lambda < 625\text{ nm}$ . The estimated average decay times are  $\langle \tau \rangle = 9.16 \pm 0.07\text{ ns}$  and  $\langle \tau \rangle = 4.87 \pm 0.05$  for the emitters in the reference (solid blue line) sample and in the structure (dashed red line), respectively.

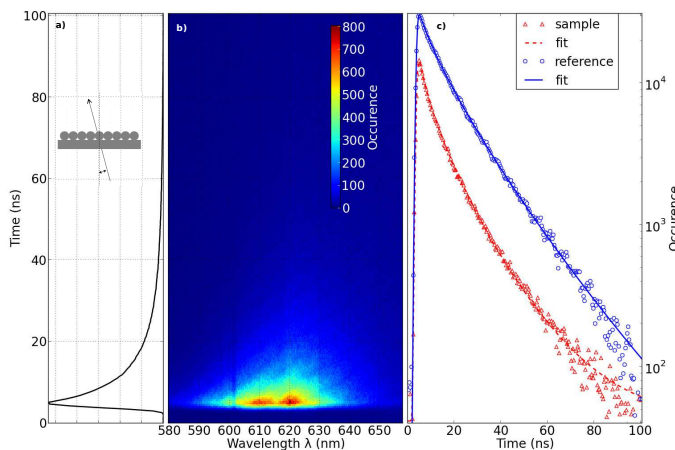


**Fig. 3** Experimental fluorescence decay profile (a) obtained by projecting on the time axis the fluorescence diagram (b) of emitters deposited onto the gold 2Dhcc structure measured at an oblique incidence  $\theta = 60^\circ$ . c) Decay profiles, for the selected 620–625 nm wavelength range, of emitters deposited either on the glass substrate (blue circles) used as a reference or on the structured sample (red triangle). The lines are the best fits of a stretched exponential function convoluted with the instrumental response function of the setup.

In order to determine the average emission rate enhancement

$\langle F \rangle$  of the CdSe@ZnS quantum dots deposited on the structure, we have divided the decay rates of the quantum emitters on the 2Dhcc structures  $\Gamma^{2Dhcc}$  with respect to the same respective emitters deposited on glass  $\Gamma^{glass}$ , according to Eq. 2<sup>41</sup>.

$$\langle F \rangle = \frac{\Gamma^{2Dhcc}}{\Gamma^{glass}} \quad (2)$$

A  $\langle F \rangle \simeq 2$  has been determined for these emitters deposited on the 2Dhcc structure within the selected wavelength range and incidence angle. This way, we determined the average emission rate enhancements for all types of emitters investigated in this paper, in wavelength ranges of 5 nm across their emission spectra. Figure 4a shows the transmission spectra of the structure at different incidence angles for unpolarized light. With an increase of  $\theta$ , the main transmission peak (BP) is indeed red-shifted and its intensity decreases. Considering the coupling condition with a reciprocal vector of a hexagonal structure<sup>31</sup> and taking into account the gold dispersion, we estimated the BP resonance wavelength by resolving eq. 1. It shifts from 595 to 680 nm.

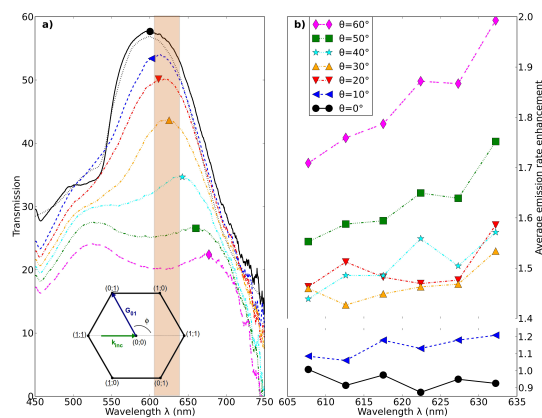


**Fig. 4** a) Experimental transmission spectra (lines) of the 2Dhcc structure for different incidence angles and unpolarized incident light. The symbols indicate the predicted wavelengths of the BP resonances. The shaded area represents the spectral emission range of the used QDs. b) Average emission rate enhancement of the 610 nm maximum CdSe@ZnS emitters as a function of wavelength for different incidence angles.

Figure 4b shows the wavelength-dependent evolution of the average emission rate enhancement. At  $\theta = 60^\circ$  incidence angle, for which the emission spectrum of the considered emitters is on the blue side of the BP mode,  $\langle F \rangle$  rises as a function of wavelength. Then, as the angle  $\theta$  is progressively reduced close to 0, dragging the transmission maximum to the short wave side through the emission spectrum, the slope of  $\langle F \rangle$  as a function of wavelength decreases progressively prior to be slightly negative at  $\theta = 0$ . As a whole, very interestingly, we do observe an

## 3 RESULTS AND DISCUSSION

asymmetric dispersive behavior of the emission rate enhancement with a relatively steep rise of  $\langle F \rangle$  while approaching the BP resonance and a smooth decline once passed.

To further demonstrate such observation of an asymmetric, non Lorentzian spectral detuning between the dipole emitter and the BP resonance frequencies, we performed additional measurements. On the one side, we manufactured 2Dhcc structures based on larger PS beads of diameters  $D = 505$  nm. After gold deposition, we dispersed a solution of 610 nm maximum CdSe@ZnS quantum emitters onto the structure. Because of the larger lattice parameter, the whole transmission spectrum of the structure is shifted to the long wave side so that the emission spectrum of the quantum dots lies on the blue side of the BP mode. Figure 5 shows the numerically (a) and experimentally (c) obtained spectra, with (red up triangles) or without (black solid line) emitters deposited on top of the structure (c), together with the emission spectrum of the latter (b). Clearly, the matching between the simulated and experimental spectra is good with a transmission maximum (absorption minimum) located at 650, 680 nm, respectively. The deposition of the quantum dots on top of the structure did not modify significantly the transmission spectrum (red curve compared to the black one in Fig. 5c), preserving the spectral matching of the short wave side of the BP mode and the QDs emission spectrum. After measurement of  $\langle F \rangle$ , according to the procedure here above described and use of Eq. 2, we observe an increase of  $\langle F \rangle$  as a function of wavelength while reaching the BP mode from the short wave side (Fig. 5d), in full agreement with the results shown in Fig. 4b.

On the other side, we have dispersed 570 and 640 nm emission maxima CdSe@ZnS quantum dots on top of the initial 2Dhcc structures (with PS beads of 457 nm diameter). These two types of quantum dots have been chosen since their emission spectra cover nicely one or the other side of the BP mode. Figure 6a shows the  $\langle F \rangle$  obtained at normal incidence for each of these emitters ( $\lambda_{max} = 570$  nm, blue squares;  $\lambda_{max} = 640$  nm, red circles). Very remarkably, the wavelength-dependent  $\langle F \rangle$  again exhibits a clear asymmetric profile.

In an attempt to understand the origin of the asymmetric line shape, we performed FDTD simulations of the photonic local density of states (LDOS) and emission rate enhancement  $F$  for single emitters in 4 different configurations. According to ref.<sup>36</sup>, the LDOS in the direction  $l \in x,y,z$  is

$$D_l(\mathbf{x}_0, \omega) = \frac{4}{\pi} \epsilon(\mathbf{x}_0) P_l(\mathbf{x}_0, \omega), \quad (3)$$

where  $P_l(\mathbf{x}_0, \omega)$  is the power radiated by an impulsive dipole current source  $\mathbf{J} = \mathbf{e}_l \delta(\mathbf{x} - \mathbf{x}_0) p(t)$ , located at  $\mathbf{x}_0$ ,  $\epsilon(\mathbf{x}_0)$  is the dielectric constant at this point and  $\mathbf{e}_l$  is the unit vector in the direction  $l$ .

In the FDTD model here employed, accumulating the Fourier transform  $\hat{E}_l(\mathbf{x}_0, \omega)$  of the field generated at  $\mathbf{x}_0$  by the

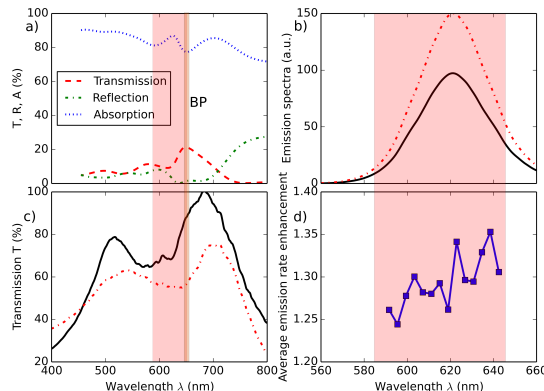


**Fig. 5** FDTD simulated transmission (T), reflection (R) and absorption (A) spectra (a) and experimental transmission spectra (c) of the 2Dhcc structure based on the CSA of 505 nm diameter beads. In c, the red dashed-dotted curve is the spectrum with emitters randomly spread on top of the structure while the black solid line is the spectrum of the bare structure. Emission spectra (b) of the 610 nm maximum emission CdSe@ZnS quantum dots spread onto either a glass substrate (black solid line) or the 2Dhcc structure (red dashed-dotted line) and the corresponding experimentally obtained  $\langle F \rangle$  (d). The shaded areas represent the spectral emission range of the used QDs.

impulsive broadband dipole current source yielded the complete LDOS spectrum  $D_l(\mathbf{x}_0, \omega) = -\frac{2}{\pi} \epsilon(\mathbf{x}_0) \frac{Re[\hat{E}_l(\mathbf{x}_0, \omega) \hat{p}(\omega)^*]}{|\hat{p}(\omega)|^2}$  at  $\mathbf{x}_0$  in a single calculation. In each chosen configuration, we computed the LDOS twice, the impulsive dipole current source mimicking the quantum emitter being close to either the 2Dhcc structure or the glass substrate taken as a reference. The emission rate enhancement  $F$  is finally obtained by dividing the LDOS in the structure with the LDOS in the reference, eq. 4<sup>41</sup>.

$$F_l(\mathbf{x}_0, \omega) = \frac{D_l^{2Dhcc}(\mathbf{x}_0, \omega)}{D_l^{glass}(\mathbf{x}_0, \omega)} \quad (4)$$

The 4 configurations we have chosen are to locate a single quantum emitter at 10 nm far from the structure/substrate either in front of a sphere or just in between two adjacent spheres, where the metallic half-shells meet. In each case, we have considered two different polarizations of the emitters:  $l \in x,z$ , with  $x$  in the plane of the substrate and  $z$  normal to it.

Figure 6b shows the wavelength-dependent emission rate enhancement for emitters located and polarized in either one of the 4 configurations here above mentioned ( $-$ ,  $|$ :  $x$  and  $z$  polarizations in front of a sphere;  $o-o$ ,  $o|o$ :  $x$  and  $z$  polarizations in between two spheres) for the 2Dhcc structure. As expected, the location of the emitter and its polarization matter. The largest  $F$  have been obtained for the emitter located in between the metallic half-shells, with  $F$  of the  $x$ -polarized emitter overwhelming by almost one order of magnitude the one of the

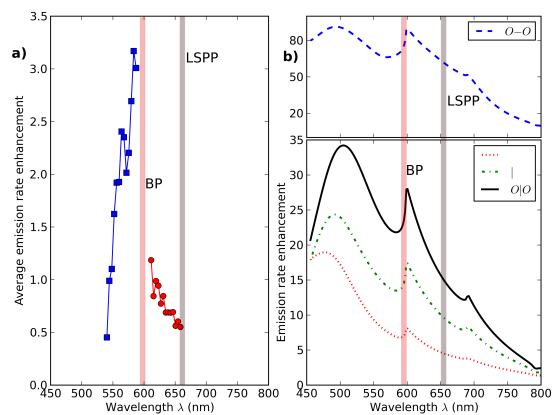


**Fig. 6** Experimentally (a) and numerically (b) determined (average  $\langle F \rangle$ ) emission rate enhancements  $F$  of emitters deposited on the 2Dhcc structure. The blue squares and red circles correspond to the measured  $\langle F \rangle$  of the CdSe@ZnS quantum dots with emission at  $\lambda_{max} = 570$  and  $\lambda_{max} = 640$  nm, respectively, deposited randomly on the structures (a). Red dotted, green dashed-dotted, black solid and blue dashed lines pertain to the simulated  $F$  of a single emitter located at 10 nm in front of the air-2Dhcc boundary either in the  $-$ ,  $|$ ,  $o-o$ , or  $o|o$  configuration (b).

z-polarized emitter. The x-polarization of the emitter at this location is indeed normal to the half-shell boundaries, a situation well known to lead to an optimized coupling between the dipole and the plasmon resonances. The simulated T, R, A spectra have shown that the BP mode occurs at  $\lambda = 595$  nm. The maximum  $F$ , which is located at precisely the same wavelength, thus marks equally well the BP resonance. For all considered configurations,  $F$  rises abruptly towards the maximum and decreases more smoothly after passing it, in an asymmetric way, dissimilar to the traditional Lorentzian spectral detuning generally expected between the emitter frequency and the resonance frequency of a single cavity<sup>1</sup>.

It is noteworthy to note here that the numerically obtained  $F$  dispersion profiles (Fig. 6b) agree well, qualitatively (in shape and not in absolute values), with the experimentally measured  $\langle F \rangle$  (Figs. 6b, 4b and 5c). Several reasons can be invoked to explain the discrepancy between these exhibited asymmetric profiles and the expected traditional Lorentzian detuning. The Purcell factor generally reported in the literature<sup>1</sup> is based on the assumption that the emitter is at the field maximum (both spectrally and spatially) and that the dipole moment orientation is parallel to the field at this point. Moreover, there is an implicit assumption that the emitter couples to a single mode only. These requirements are not fulfilled in our numerical implementation. Indeed, the emitters are placed at positions that agree with the experimental conditions (10 nm far from the surface). They neither are located at positions of field maximum nor have a polarization strictly parallel to the field. Furthermore

and most importantly, the simulations are not performed in the single mode regime. Other modes (e.g. LSPP) are spectrally close and the Bragg-plasmon mode in itself consists in the hybridization between a plasmonic and a photonic mode. Such a hybridized mode is likely to influence the emission properties of a quantum emitter weakly coupled to it in a way different as would do a traditional single cavity mode.

Experimentally, the situation is complicated by the fact that many emitters are measured simultaneously. Indeed, in the experiments, the emitters are spread onto the samples from a solution. They are thus dispersed everywhere on the sample with their dipole moments randomly oriented. The measurements thus lead to an emission rate enhancement  $\langle F \rangle$  averaged over spatial positions and polarizations, where quasi-static corrections add in an asymmetry that is well beyond the Purcell factor regime. The emission rate enhancement determined theoretically  $F$  and experimentally  $\langle F \rangle$  are thus not strictly comparable and an averaging process, depending on all positions, dipole moment orientations and emission frequencies of the  $N$  emitters must be considered. This explains the quantitative differences observed in Fig. 6b between the amplitudes of the experimental  $\langle F \rangle$  and simulated  $F$ .

## 4 Conclusion

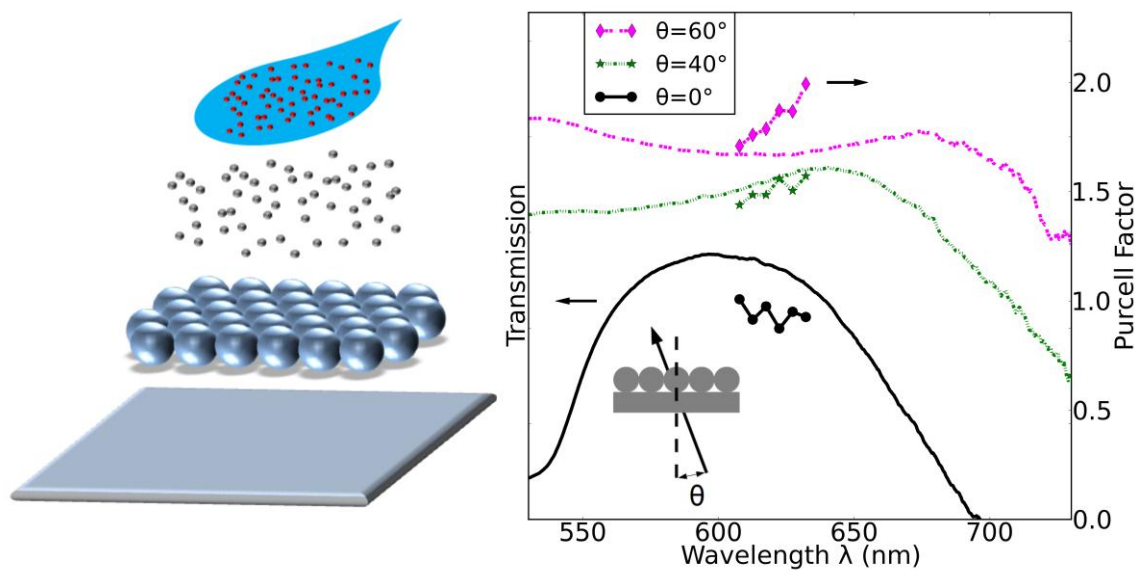
In conclusion, we have designed several types of hybrid metallo-dielectric structures, by combining commensurate PS colloidal mono-layers and gold over-layers. Specific plasmo-photonic modes appear, which are well-signaled in the UV-visible transmission spectra. The proper assignment of these modes has been performed owing to extensive comparison of the experiments with FDTD simulations. Focusing specifically on the Bragg-plasmon (BP) mode of the various structures, we have measured and simulated the wavelength-dependent emission rate enhancement  $F$  of emitters spread on top of the structures. We found truly appealing the fact that both numerical and experimental findings reveal that the spectral dependence of  $F$  is non Lorentzian. The dominant aspect of this behavior has been attributed to the fact that a hybridized mode, not a pure single mode, is affecting the emission properties of the quantum emitters. The full understanding of emission detuning by hybrid plasmonic/photonic structures exceeds pure academic interest and would provide benefits in many related fields. Notably, a full understanding would require a more detailed study in order to correlate not only spectral overlapping but mainly spatial overlapping, which in turn plays the fundamental role in most light matter interaction mechanisms. We consider single molecule spectroscopy<sup>35</sup> as the most suitable technique to reach this goal. Furthermore, these studies could lead to advancement in sensing and biosensing technologies, with the observation of a  $F$  asymmetric dispersion profile as a potential sensing trace of a hybridized mode.

## 5 Acknowledgment

The authors acknowledge le Conseil Régional d'Aquitaine for the experimental financing support and the allowance of a post-doctoral fellowship to S. Ungureanu. Pierre Fauché acknowledges a Ph. D fellowship from the LabEx LAPHIA. B. Kolaric acknowledges the financial support from both Smart film grant 830039 (ECV12020020892F) in the framework of the Convergence Project and FNRS. R. Vallée acknowledges FRS-FNRS for a visiting professor grant.

## References

- 1 E. M. Purcell, *Phys. Rev.*, 1946, **69**, 681.
- 2 E. Yablonovitch, *Phys. Rev. Lett.*, 1987, **58**, 2059–2062.
- 3 P. Lodahl, A. Floris Van Driel, I. S. Nikolaev, A. Irman, K. Overgaag, D. Vanmaekelbergh and W. L. Vos, *Nature*, 2004, **430**, 654–657.
- 4 R. A. L. Vallée, K. Baert, B. Kolaric, M. Van der Auweraer and K. Clays, *Phys. Rev. B*, 2007, **76**, 045113.
- 5 S. Noda, M. Fujita and T. Asano, *Nat. Photonics*, 2007, **1**, 449–458.
- 6 K. Aoki, D. Guimard, M. Nishioka, M. Nomura, S. Iwamoto and Y. Arakawa, *Nat. Photonics*, 2008, **2**, 688–692.
- 7 M. Khajavikhan, A. Simic, M. Katz, J. H. Lee, B. Slutsky, A. Mizrahi, V. Lomakin and Y. Fainman, *Nature*, 2012, **482**, 204–7.
- 8 T. H. Tamimiau, F. D. Stefani, F. B. Segerink and N. F. van Hulst, *Nat. Photonics*, 2008, **2**, 234–237.
- 9 L. Novotny and N. van Hulst, *Nat. Photonics*, 2011, **5**, 83–90.
- 10 M. A. Noginov, G. Zhu, A. M. Belgrave, R. Bakker, V. M. Shalaev, E. E. Narimanov, S. Stout, E. Herz, T. Suteewong and U. Wiesner, *Nature*, 2009, **460**, 1110–2.
- 11 R. F. Oulton, V. J. Sorger, T. Zentgraf, R.-M. Ma, C. Gladden, L. Dai, G. Bartal and X. Zhang, *Nature*, 2009, **461**, 629–32.
- 12 J. T. Choy, B. J. M. Hausmann, T. M. Babinec, I. Bulu, M. Khan, P. Maletinsky, A. Yacoby and M. Lončar, *Nat. Photonics*, 2011, **5**, 738–743.
- 13 X. Yang, A. Ishikawa, X. Yin and X. Zhang, *ACS Nano*, 2011, **5**, 2831–2838.
- 14 B. Lamprecht, G. Schider, R. T. Lechner, H. Ditlbacher, J. R. Krenn, A. Leitner and F. R. Aussenegg, *Phys. Rev. Lett.*, 2000, **84**, 4721–4724.
- 15 B. Auguie and W. L. Barnes, *Phys. Rev. Lett.*, 2008, **101**, 143902.
- 16 M. Ferrié, N. Pinna, S. Ravaine and R. A. L. Vallée, *Opt. Express*, 2011, **19**, 17697–17712.
- 17 R. A. L. Vallée, M. Ferrié, H. Saadaoui and S. Ravaine, *Opt. Mater. Express*, 2012, **2**, 566–577.
- 18 S. Ungureanu, B. Kolaric, J. Chen, R. Hillenbrand and R. A. L. Vallée, *Nanophotonics*, 2013, **2**, 173–185.
- 19 M. Ringler, A. Schwemer, M. Wunderlich, A. Nichtl, K. Kürzinger, T. Klar and J. Feldmann, *Phys. Rev. Lett.*, 2008, **100**, 203002.
- 20 S. G. Romanov, A. V. Fokin and R. M. De La Rue, *Appl. Phys. Lett.*, 1999, **74**, 1821.
- 21 B. Ding, C. Hrelescu, N. Arnold, G. Isic and T. A. Klar, *Nano Lett.*, 2013, **13**, 378–386.
- 22 J. N. Anker, W. P. Hall, O. Lyandres, N. C. Shah, J. Zhao and R. P. Van Duyne, *Nat. Mater.*, 2008, **7**, 442–453.
- 23 A. V. Kabashin, P. Evans, S. Pastkovsky, W. Hendren, G. A. Wurtz, R. Atkinson, R. Pollard, V. A. Podolskiy and A. V. Zayats, *Nat. Mater.*, 2009, **8**, 867–871.
- 24 H. A. Atwater and A. Polman, *Nat. Mater.*, 2010, **9**, 205–213.
- 25 C. Clavero, *Nat. Photonics*, 2014, **8**, 95–103.
- 26 U. C. Fischer and H. P. Zingsheim, *J. Vac. Sci. Technol.*, 1981, **19**, 881–885.
- 27 J. C. Hultheen and R. P. Van Duyne, *J. Vac. Sci. Technol. A*, 1995, **13**, 1553.
- 28 J. C. Hultheen, D. A. Treichel, M. T. Smith, M. L. Duval, T. R. Jensen and R. P. Van Duyne, *J. Phys. Chem. B*, 1999, **103**, 3854–3863.
- 29 C. L. Haynes and R. P. Van Duyne, *J Phys Chem B*, 2001, **105**, 5599–5611.
- 30 R. Morarescu, H. Shen, R. a. L. Vallée, B. Maes, B. Kolaric and P. Damman, *J. Mater. Chem.*, 2012, **22**, 11537.
- 31 L. Landström, N. Arnold, D. Brodoceanu, K. Piglmayer and D. Bäuerle, *Appl. Phys. A*, 2006, **83**, 271–275.
- 32 P. Zhan, Z. L. L. Wang, H. Dong, J. Sun, J. Wu, H.-T. Wang, S. N. N. Zhu, N. B. B. Ming and J. Zi, *Adv. Mater.*, 2006, **18**, 1612–1616.
- 33 S. G. Romanov, A. V. Korovin, A. Regensburger and U. Peschel, *Adv. Mater.*, 2011, **23**, 2515–2533.
- 34 C. Farcau, M. Giloan, E. Vinteler and S. Astilean, *Appl. Phys. B*, 2012, **106**, 849–856.
- 35 A. Kinkhabwala, Z. Yu, S. Fan, Y. Avlasevich, K. Müllen and W. E. Moerner, *Nat. Photonics*, 2009, **3**, 654–657.
- 36 *Advances in FDTD Computational Electrodynamics: Photonics and Nanotechnology*, ed. A. Taflov, A. Oskooi and S. G. Johnson, Artech House, Inc., 2013.
- 37 A. D. Rakic, A. B. Djurišić, J. M. Elazar and M. L. Majewski, *Appl. Opt.*, 1998, **37**, 5271–5283.
- 38 W. L. Barnes, W. A. Murray, J. Dintinger, E. Devaux and T. W. Ebbesen, *Phys. Rev. Lett.*, 2004, **92**, 107401.
- 39 L. Landström, D. Brodoceanu, D. Bäuerle, F. J. Garcia-Vidal, S. G. Rodrigo and L. Martin-Moreno, *Opt. Express*, 2009, **17**, 761–772.
- 40 L. Landström, D. Brodoceanu, K. Piglmayer and D. Bäuerle, *Appl. Phys. A*, 2006, **84**, 373–377.
- 41 M. Agio, *Nanoscale*, 2012, **4**, 692–706.

Table of contents

Scheme of the hybrid plasmo-photonic structure manufacturing process - Angular transmission spectra and asymmetric emission rate enhancement of the deposited QDs.